DOI: https://doi.org/10.2138/am-2019-6771

Revision 2

Influence of aluminum on the elasticity of majorite-pyrope garnets

Zhaodong Liu [1, 2 *], Steeve Gréaux [3], Nao Cai [4], Nicki Siersch [1], Tiziana Boffa Ballaran [1], Tetsuo Irifune [3], Dan J. Frost [1]

1. Bayerisches Geoinstitut, University of Bayreuth, 95440 Bayreuth, Germany
2. State Key Laboratory of Superhard Materials, Jilin University, Changchun 130012, China
3. Geodynamics Research Center, Ehime University, Matsuyama 790-8577, Japan
4. Mineral Physics Institute, Stony Brook University, Stony Brook, NY 11794, USA

* Corresponding author: Zhaodong Liu (lzd.0520@163.com)

ABSTRACT

The effect of aluminum (Al) on the elasticity of majorite-pyrope garnets was investigated by means of ultrasonic interferometry measurements on well-fabricated polycrystalline specimens. Both velocities and elastic moduli increase almost linearly with increasing Al content within analytical uncertainty. No significant variation of the velocities and elastic moduli is observed across the tetragonal-to-cubic phase transition at majorite with the pyrope content up to 26 mol% along the majorite-pyrope system. The elasticity variation of majorite-pyrope garnets is largely dominated by the Al content, while the phase transition as a result of cation ordering/disordering of Mg and Si via substitution of Al on octahedral sites cannot significantly affect elastic properties. Seismic velocity variations of a garnet-bearing mantle transition zone are therefore dominated by garnet composition (e.g., Al, Fe, Ca, and Na) rather than the tetragonal-to-cubic phase transition because of cation ordering/disordering.

Keywords: aluminum, garnet, phase transition, velocity, elastic modulus, mantle transition zone

INTRODUCTION

Garnet, $X_3Y_2Si_3O_{12}$ (where X^{2+} = Mg, Fe, Ca, and Mn in a dodecahedral site; Y^{3+}= Al, Fe, and Cr in the octahedral site), is one of the most abundant rock-forming minerals in the Earth's crust and mantle (*e.g.*, Novak and Gibbs 1971; Ringwood and Major 1971; Anderson and Bass, 1986). With increasing depths from the upper mantle to the mantle transition zone, an aluminum deficient garnet called majorite forms from the gradual dissolution of clinopyroxenes into the garnet (Ringwood and Major 1971). Petrological studies have demonstrated that majoritic garnets represent up to 40% and 60% by volume of pyrolite and mid-ocean ridge basalt (MORB) compositions in the mantle transition zone, respectively. Mantle garnets are a solid solution with complex chemical compositions within the Mg-Ca-Fe-Cr-Al-Si-O system (Novak and Gibbs 1971; Ringwood and Major 1971; Irifune and Ringwood, 1987). The majorite ($MgSiO_3$)-pyrope ($Mg_3Al_2Si_3O_{12}$) system is considered the most relevant to the upper mantle and transition zone (*e.g.,* Irifune and Ringwood, 1987). Accordingly, the physical and chemical properties of majorite-pyrope garnets are indispensable for constructing the mineralogy of the Earth's mantle.

An increase of pyrope content to 25 mol% ($Mj_{75}Py_{25}$, Mj: majorite; Py: pyrope) in majorite leads to a phase transition from a tetragonal ($I4_1/a$) to cubic ($Ia\bar{3}d$) symmetry along the majorite-pyrope system, which is caused by the effect of cation disordering of Mg and Si on two distinct octahedral sites after Al substitution (Heinemann et al., 1997; Liu et al., 2016; Parise et al., 1996). Because of its potential ferroelastic properties, former studies speculated that the tetragonal-to-cubic transition in majoritic garnets may explain observed seismic scatterings in the mantle transition zone (Heinemann et al. 1997). Although the elastic properties of majorite-pyrope garnets have been widely studied by Brillouin spectroscopy (*e.g.*, Bass and Kanzaki, 1990; Yeganeh-Haeri et al., 1990; Pacalco and Weidner, 1997; Sinogeikin et al., 1997, 2002a, 2002b; Pamato et al., 2016) and ultrasonic interferometry (Rigden et al., 1994; Liu et al., 2000; Gwanmesia et al., 2000, 2006, 2009; Zou et al., 2012; Liu et al., 2015; Chantel et al., 2016), the dependence of their elasticity on chemistry remains controversial. Sinogeikin et al. (1997) proposed two models to explain the variation of elastic moduli as a function of the pyrope content in this system: (1) a small linear decrease of K_S (bulk modulus) and G (shear modulus) from pyrope to majorite; (2) constant K_S and G from pyrope to $Mj_{70}Py_{30}$, followed by a step-like decrease at $Mj_{80}Py_{20}$ and a gradual increase to majorite. The latter model was proposed based on earlier results reported by Bass and Kanzaki (1990), Yeganeh-Haeri et al. (1990), and Pacalo and Weidner (1997). However, these data are relatively scattered due to different sample qualities and experimental techniques. It thus cannot draw a firm conclusion about the scattering nature of the compositional dependency of garnet's elastic moduli. Furthermore, potential effects of the tetragonal-to-cubic symmetry transformation on garnet's elastic moduli also remain unclear. Therefore, it is required to clarify the effect of Al content on the elasticity of majorite-pyrope garnets.

In this study, we investigated the variation of P- and S-wave velocities and elastic moduli of a series of majorite-pyrope garnets using ultrasonic measurements. All samples were synthesized under nearly identical pressure and temperature conditions using a Kawai-type multi-anvil apparatus. Based on our new results, we quantify the effect of Al on the elasticity of majorite-pyrope garnets and discuss the contribution of garnet composition to the velocity profile of the mantle transition zone.

EXPERIMENTAL METHODS

Single-phase and well-sintered polycrystalline Mj_xPy_{100-x} garnets (x mol% majorite and (100-x) mol% pyrope; x = 100, 90, 80, 74, 59, 20, and 0) were synthesized by hot-pressing glass starting material at 18 GPa and 2000 K for 2 hours in a Kawai-type multi-anvil apparatus with a press load of 3000 tons at the Geodynamics Research Center, Ehime University and Sumitomo-1200 with a press load of 1200 tons at the Bayerisches Geoinstitut, University of Bayreuth, Germany. A detailed description of the sample synthesis and characterization is reported in our recent study (Liu et al., 2017), in which the same stock of samples was used. Recovered samples were transparent or translucent and free of microcracks (**Fig.1**), showing equilibrated textures and homogeneous compositions of grains with a size of 1-2 μm (see Liu et al., 2017). We ground one typical cubic ($Mj_{59}Py_{41}$) and one tetragonal ($Mj_{90}Py_{10}$) garnet for characterization by powder X-ray diffraction (XRD) characterization (**Fig. 2)**. The densities

($\rho_{M59Py41}$ =3.537 ± 0.006g/cm^3, $\rho_{Mj90Py10}$ = 3.522 ± 0.008g/cm^3) are practically identical to those derived previously by Micro XRD ($\rho_{M59Py41}$ =3.546 ± 0.008g/cm^3, $\rho_{Mj90Py10}$ = 3.530 ± 0.007 g/cm^3 ; Liu et al., 2017). The bulk densities of $Mj_{59}Py_{41}$ and $Mj_{90}Py_{10}$ garnets were also determined by Archimedes' method with 0.2% uncertainty compared with those obtained from XRD, suggesting a very low porosity. The densities of garnets were therefore derived from their unit cell volumes measured using the same instrument in our recent study (Liu et al. 2017).

We measured travel times of *P*- and *S*-waves through the garnet specimens under ambient conditions by the pulse echo overlap method (Li et al., 2002). The ends of each sample were polished into parallel mirror surfaces using 0.25 μm diamond pastes. *P*- and *S*-wave acoustic signals were generated by a 10º Y-cut $LiNbO_3$ piezoelectric transducer, which was attached at one end of a SiO_2 glass rod by a very trace amount of low-viscosity epoxy bond. The glass rod was served as a delay line buffer of the signal into the specimen. The other end of sample was covered by a thin gold foil with a thickness of 2 μm to improve the mechanical coupling and then one teflon disk to protect the sample. As shown in **Fig.1**, the sample of $Mj_{90}Py_{10}$ garnet was attached to the other end of the glass buffer rod using a very trace amount of low-viscosity epoxy bond. The effect of epoxy bond on the travel time can be ignored because of a very trace amount and easily dispersing under a very low press load. Each sample was measured for two or three times. Although the travel times of several samples ($Mj_{90}Py_{10}$ and $Mj_{80}Py_{20}$) have some frequency dependences below 50 MHz for P-wave but become independent with frequencies above 50 MHz. Most samples (Mj_{100}, $Mj_{59}Py_{41}$, $Mj_{74}Py_{26}$, $Mj_{20}Py_{80}$ and Py_{100}) show not a clear frequency dependence for the travel time (see Supplemental **Fig. S1**). This situation may be related with the quality of attaching $LiNbO_3$ transducers on the surface of the buffer rod due to a slightly different temperature or press load. In the present study, we collected travel times from 25 to 60 MHz for all the samples. In order to minimize analytical uncertainties, we therefore derived the travel time of P- and S-wave at the highest resonant frequencies of 60 and 40 MHz, respectively. Its acoustic signals obtained at 60 MHz (P-wave) are shown at the bottom of **Fig.1.** The echo at the interface between the buffer rod and sample ($B1$) was followed by four successive echoes from the other end of the garnet sample ($P1$, $P2$, $P3$, and $P4$ for

P-waves). The two-ways travel times of acoustic waves were obtained by measuring the time delay between echoes *(B1)* and *(P1),* while the sample length was measured using a micrometer with a resolution of 0.001 mm before the ultrasonic measurements.

RESULTS and DISCUSSION

Phase transition and density

XRD patterns of one typical cubic ($Mj_{59}Py_{41}$) and one tetragonal ($Mj_{90}Py_{10}$) garnet, respectively, obtained under ambient conditions verify that each sample consists of a single garnet phase (**Fig.2**). XRD reflections of the $Mj_{59}Py_{41}$ garnet can be assigned to a cubic structure ($Ia\bar{3}d$), while those of $Mj_{90}Py_{10}$ correspond to a tetragonal structure ($I4_1/a$). The main diffraction pattern differences between these two structures are the appearance of new peaks (e.g., (222) and (0kl) where k, l = 2n) and the splitting of cubic diffraction peaks (e.g., (h00) and (hhl)) for tetragonal garnets. In general, most diffraction peaks of the tetragonal garnet are heavily overlapping doublets, triplets, or combinations compared with those of cubic garnet. More detailed differences between these two garnet structures are described in previous studies (Parise et al., 1996; Heinemann et al., 1997; Liu et al., 2017), which showed that the phase transition from tetragonal to cubic occurs in majoritic garnets with the pyrope content smaller than 26 mol% because of the increasing degree of Mg and Si ordering on the octahedral sites with decreasing Al content. Although the structure distortion of Al-depleted tetragonal majoritic garnets is related to the degree of the order/disorder of Mg and Si on octahedral sites due to the substitution of different size cations (Mg = 0.72 Å, Si = 0. 40 Å, and Al = 0.535 Å, Shannon, 1976) (**Fig. 3**), the incorporation of Al tends to stabilize the cubic structure.

Fig. 3 shows the density of majorite-pyrope garnets obtained in this study as a function of the pyrope content alongside previously reported data (Bass and Kanzaki, 1990; Parise et al., 1996; Heinemann et al., 1997; Sinogeikin et al., 1997; Liu et al., 2000; Gwanmesia et al., 2000, 2006, 2009; Pamato et al., 2016). Our results are in agreement with most previous studies within the mutual analytical uncertainty and show a linear dependence of density on the pyrope content. Data reported by Sinogeikin et al. (1997) are significantly higher than our and other earlier

DOI: https://doi.org/10.2138/am-2019-6771

studies, which may be related to different synthesis conditions and measurement methods between the former and latter studies. Nevertheless, a linear function was used to fit the present data, yielding the following equation (the detailed fitting can be found in Supplemental Figure S2):

$$\rho = 3.524\ (3) + 4.54\ (61) \cdot 10^{-4} \cdot X_{Py} \tag{1}$$

where X_{py} is the pyrope content in mole percent (mol%) and the numbers in parentheses represent the standard deviation of the last digit. This linear composition dependence of density can be explained by an increase of cation radius from 0.535 Å of Al to 0.56 Å of (Mg+Si)/2 on octahedral sites of the garnet structure (Shannon, 1976). In contrast, the phase transition from a tetragonal to cubic symmetry does not significantly affect the density variation because the cubic end-member pyrope is only 1 % less dense than that of the tetragonal end-member majorite (Parise et al., 1996; Heinemann et al., 1997; Liu et al., 2015, 2017).

Elasticity

Fig. 4a shows the acoustic compressional wave (V_P) and shear wave (V_S) velocities of the garnets under ambient conditions measured by Brillouin scattering and ultrasonic interferometry measurements in the present and previous studies. We found that both V_P and V_S have a linear dependence on the pyrope content in the present study, which is generally consistent with earlier studies except for the values of majorite and $Mj_{33}Py_{67}$ obtained by Pacalo and Weidner (1997) and Yeganeh-Haeri et al. (1990), respectively, using Brillouin spectroscopy. These velocities are obviously faster than values obtained in the present study for the garnet with the same composition. This difference may be caused by the different measurement methods and sintering quality of the samples. For example, the grain size of sintering samples in Yeganeh-Haeri et al. (1990) was around 8 μm, which is significantly higher than that in our study (3 μm). Smaller-grained samples have a better sintering quality, which reduces wave dispersive effects. Thus, the same elastic wave measurement technique on the high-quality sintering specimens is critical for constraining the compositional dependence of elasticity due to substantially reduced analytical uncertainties.

Adiabatic bulk (K_S) and shear (G) moduli (**Table 1**) were derived from the experimental densities and acoustic *P*- and *S*-wave velocities using the following equations:

$$K_S = \rho \cdot (V_p^2 - 4V_s^2/3) \tag{2}$$

$$G = \rho \cdot V_s^2 \tag{3}$$

Fig. 4b shows K_S and G values obtained here compared with previous studies. Our results show a monotonic increase of K_S and G with increasing pyrope content from the majorite to pyrope. This result agrees well with a linear compositional dependence model (Bass and Kanzaki, 1990; Gwanmesia et al., 2000) rather than the model that proposed a sudden jump of K_S and G at $Mj_{70}Py_{30}$-$Mj_{80}Py_{20}$ related to the tetragonal-to-cubic phase transition (Sinogeikin et al., 1997). Different synthesis conditions, quench histories, and analytical uncertainties in previous studies have hindered a proper description of the dependency of the elastic moduli on the composition of garnet. The quality of synthetic garnets can also greatly affect the velocity measurements at ambient conditions because micro-pores or -cracks in a poorly sintering sample can result in elastic wave dispersion (Gwanmesia et al. 2000). Differences in synthesis conditions and analytical techniques therefore lead to a scattering of data from previous elasticity studies. In the present study, we synthesized high-quality majorite-pyrope garnets under nearly identical pressure and temperature conditions. Weighted least-squares fits of our data result in the following relationships for elastic moduli as a function of the pyrope content (the fitting can be found in Supplemental Figure S2):

$$K_S = 157.8\ (6) + 0.13\ (1) \cdot X_{Py} \tag{4}$$

$$G = 82\ (1) + 0.10\ (2) \cdot X_{Py} \tag{5}$$

The value of the slope (S) of K_S in the present study is relatively lower and higher, respectively, than that obtained by Bass and Kanzaki (1990) (S_{Ks}= 0.22) and Gwanmesia et al. (2000) (S_{Ks}= 0.085), while that of G is slightly higher than that obtained in latter two studies (Bass and Kanzaki, 1990: S_G=0.06; Gwanmesia et al. 2000: S_G=0.038). These differences can be explained by the fact that only two samples were measured in the latter two studies compared with a series

DOI: https://doi.org/10.2138/am-2019-6771

of samples in the present study.

Our results clearly show that the tetragonal-to-cubic phase transition does not affect garnet density nor velocity in the majorite-pyrope system and thereby cannot result in large differences in elastic moduli when the phase transition occurs. This result is consistent with the first-principles simulations by Li et al (2007), who proposed that cation-ordering has a smaller effect than compositional changes (i.e., the Al incorporation) because volume and bulk modulus are independent of the degree of cation ordering/disordering. Model (2) of Sinogeikin et al. (1997) was derived from the measurements of only three garnets, whereas here we systematically investigated a series of majorite-pyrope garnets and therefore can precisely constrain on the effect of cation substitution on elastic modulus. Based on our new experimental results, we reconcile the discrepancies in previously reported results and propose that Al plays a dominant role in the variation of garnet elasticity in the majorite-pyrope system.

IMPLICATIONS

Our study shows a quasi-monotonic increase of velocity and elastic modulus as a function of the pyrope content along the majorite-pyrope system. The tetragonal-to-cubic phase transition because of cation ordering/disordering cannot significantly affect the variation of sound velocity and elastic modulus, suggesting that Al component plays a more dominant role. Accordingly, seismic velocity modelling of a garnet-bearing mantle needs only to address garnet composition (e.g., Al, Ca, and Fe) rather than the tetragonal-to-cubic phase transition. As shown in **Fig.5a**, both bulk and shear moduli of majorite-pyrope garnets are comparable to those of majorite-almandine ($Fe_3Al_2Si_3O_{12}$) garnets (Wang and Ji, 2001; Arimoto et al., 2015). The bulk moduli of grossular ($Ca_3Al_2Si_3O_{12}$) garnet (171 GPa) obtained by Kono et al. (2010) and Gwanmesia et al. (2014) fall within the range of those of majorite-pyrope garnets (158-170 GPa) in our study, in contrast, their shear moduli (108 GPa) are significantly higher than those in the present study (80-90 GPa). Ca incorporation can therefore considerably increase the shear elasticity of mantle garnets. This fact is compatible with the relatively high shear modulus of pyrolitic majorite (95 GPa, Irifune et al., 2008) and Mid-Ocean Ridge Basalt (MORB) majorite (101 GPa, Kono et al., 2007) compared with that of majorite-pyrope garnets (82-90 GPa) because these garnets contain 3-9 wt.% CaO above ~560 km depths.

Fig.5b shows V_P and V_S of majorite-pyrope garnets (ambient conditions, this study), pyrope (Gwanmeia et al., 2006; Zou et al., 2012; Chantel et al., 2016), $Mj_{80}Py_{20}$ (Liu et al., 2015), majorite (Zhou et al., 2014), grossular (Kono et al., 2010, Gwanmeia et al., 2014), almandine (Arimoto et al., 2015), and pyrolitic majorite (Irifune et al., 2008) at high pressures. Although the almandine shows slightly higher elastic modulus than that of majorite-pyrope garnets, its corresponding V_P and V_S are generally lower by 4-8% compared to those of majorite-pyrope garnets due to its higher density (4.32 g/cm^3) than the latter garnets (**Fig.5b**), suggesting incorporation of Fe^{2+} would decrease velocities. In contrast, V_P and V_S of grossular reported by Kono et al. (2010) are substantially higher than those of the majorite-pyrope garnets (Zou et al., 2012; Gwanmeia et al., 2006, Liu et al., 2015, Zhou et al., 2014, Chantel et al., 2016) by 2-6% and 6-8 %, respectively. However, both V_P and V_S of pyrolitic majorite (Irifune et al., 2008) are within those of majorite and pyrope garnets at high pressures, suggesting that chemical variations of majorite garnets within the pyrolite-MORB joint compositions are not sufficient to explain the high seismic velocities at the bottom of the mantle transition zone.

Irifune et al. (2008) have indeed demonstrated that shear wave velocities of pyrolitic majorite are significantly lower than seismic reference models (Dziewonski and Anderson, 1981) at the base of the mantle transition zone. As a result, it is difficult to reconcile the observed seismic velocities with those of the pyrolite model at average mantle temperatures (Irifune et al., 2008; Pamato et al., 2016), despite the high velocities of the dominant mineral ringwoodite (Higo et al., 2008) and the formation of ~7-10 vol.% $CaSiO_3$ perovskite at depths below 560 km (Gréaux et al., 2019). One possible explanation for this velocity anomaly is that the composition of the lower mantle transition region may be different with the upper and middle regions. Recent studies suggested the basaltic component of the subducted slab is likely to descend into the lower mantle (Kono et al., 2012; Gréaux et al., 2019) while the remaining ultramafic component (harzburgite) would lie down at the bottom of the mantle transition zone. Such mechanical mixture of pyrolite and harzburgite components may explain velocities at these depths because the ultramafic component would contain much less garnet than the pyrolite mantle. Nevertheless, the variation of garnet composition could be an alternative for understanding the multiple seismic scattering in this region (Deuss et al., 2006; Jenkins et al., 2016). The garnet in the harzburgite layer is more majoritic (i.e., garnet composition is rich in Mg and Si and less in Al) than the ambient mantle, which could promote locally low velocity anomalies at the depths of the high velocity region (~520-660 km depths). Therefore, further study on the effect of other major cations such as Ca and Na impurities on the elasticity of majoritic garnets may provide more insights to clarify these issues.

ACKNOWLEDGMENTS

The authors thank C. Zhou and Y. Zhou for their valuable suggestions and R. Huang for her helps in XRD measurements. The manuscript is greatly improved by the constructive comments by two anonymous reviewers and the editorial handling by Z. Jing. Z. L. acknowledges 2016 PRIUS program of Ehime University. Z. L. was financially supported by the Bayerisches Geoinstitut Visitor's Program. N. C. acknowledges support from the National Science Foundation grant EAR1524078.

Reference

Anderson, D. L., and Bass, J. D. (1986) Transition region of the Earth's upper mantle, Nature, 320, 321–328.

Angel, R. J., Finger, L. W., Hazen, R. M., Kanzaki, M., Weidner, D. J., Liebermann, R. C., and Veblen, D. R. (1989) Structure and twinning of single-crystal $MgSiO_3$ garnet synthesized at 17 GPa and 1800°C. American Mineralogist, 74, 509–512.

Arimoto, T., Gréaux, S., Irifune, T., Zhou, C., and Higo, Y. (2015) Sound velocities of $Fe_3Al_2Si_3O_{12}$ almandine up to 19 GPa and 1700 K, Physics of the Earth and Planetary Interiors, 246, 1-8.

Bass, D. J., and Kanzaki, M. (1990) Elasticity of majorite-pyrope solid solution, Geophysical Research

Letters, 17, 1989-1992.

Brown, J. M. and Shankland, T. J. (1981) Thermodynamic parameters in the Earth as determined from seismic profiles. Geophysical Journal of the Royal Astronomical Society banner, 66, 579-596.

Chantel J., G. Manthilake M., Frost D. J., Beyer C., Ballaran T. B., Jing Z., and Wang Y., (2016) Elastic wave velocities in polycrystalline $Mg_3Al_2Si_3O_{12}$-pyrope garnet to 24 GPa and 1300 K, American Mineralogist, 101(4) , 991–997.

Deuss, A., Redfern, S.A.T., Chambers, K., et al. (2006). The nature of the 660-kilometer discontinuity in earth's mantle from global seismic observations of PP precursors. Science 311, 198–210.

Dziewonski, A. M. and Anderson, D. L. (1981) Preliminary reference Earth model, Physics of the Earth and Planetary Interiors 25, 297-356.

Gréaux, S., Irifune, T., Higo, Y., Tange, Y., Arimoto, T., Liu, Z., and Yamada, A. (2019) Sound velocity of CaSiO3 perovskite suggests the presence of basaltic crust in the Earth's lower mantle, *Nature* 565, 218–221.

Gwanmesia, G. D., Liu, J., Chen, G. S., Kesson, S. ,Rigden, M., and Liebermann, R. C. (2000) Elasticity of pyrope ($Mg_3Al_2Si_3O_{12}$) - majorite ($Mg_4Si_4O_{12}$) garnet solid solution, Physics and Chemistry of Minerals, 27, 445-452.

Gwanmesia, G. D., Zhang, J., Darling, K., Kung, J., Li, B., Wang, L., Neuville, D., and Liebermann, R. C. (2006) Elasticity of Polycrystalline Pyrope ($Mg_3Al_2Si_3O_{12}$) to 9 GPa and 1000°C, Physics of the Earth and Planetary Interiors, 155, 179-190.

Gwanmesia, G. D., Wang, L. Heady , A., and Liebermann, R. C. (2009) Pressure and temperature dependence of the elasticity of pyrope-majorite [$Py_{60}Mj_{40}$ and $Py_{50}Mj_{50}$] garnets solid solution measured by ultrasonic interferometry technique, Physics of the Earth and Planetary Interiors, 179: 87–95.

Gwanmesia, G. D., Wang, L., Heady, A., and Liebermann, R. C. (2014) Elasticity and sound velocities of polycrystalline grossular garnet ($Ca_3Al_2Si_3O_{12}$) at simultaneous high pressures and high temperatures. Physics of the Earth and Planetary Interiors, 228, 80–87.

Hazen, R. M., and Finger, L. W. (1978) Crystal structures and compressibility of Pyrope and Grossular to 60 kbar, American Mineralogist, 63, 297-303.

Heinemann, S., Sharp T.G., Seifert, F., and Rubie, D. C. (1997) The cubic-tetragonal phase transition in the system majorite ($Mg_4Si_4O_{12}$) - pyrope ($Mg_3Al_2Si_3O_{12}$) and garnet symmetry in the earth's transition zone. Physics and Chemistry of Minerals, 24, 206-221.

Higo, Y., Inoue, T., Irifune, T., Funakoshi, K., Li, B. (2008). Elastic wave velocities of $(Mg_{0.91}Fe_{0.09})_2SiO_4$ ringwoodite under P–T conditions of the mantle transition region. Physics of the Earth and Planetary Interiors, 166, 167–174.

Hunt, S.A., Dobson, D.P., Li, L., Weidner, D. J., and Brodholt, J. P. (2010) Relative strength of the pyrope–majorite solid solution and the flow-law of majorite containing garnets. Physics of the Earth and Planetary Interiors, 179: 87–95.

Irifune, T., and Ringwood, A. E. (1987) Phase transformations in primitive MORB and pyrolite compositions to 25 GPa and some geophysical implications. In M.H.Manghnani and Y.Syono, Eds., High Pressure Research in Mineral Physics, 231–242. Terra Scientific, Tokyo.

Irifune, T., Y. Higo, Inoue, T., Kono, Y., Ohfuji, H., and Funakoshi, K. (2008) Sound velocities of majorite garnet and the composition of the mantle transition region, *Nature*, *451*(7180), 814-817.

Jenkins, J., S. Cottaar, R. S. White, and A. Deuss (2016), Depressed mantle discontinuities beneath Iceland: Evidence of a garnet controlled 660 km discontinuity. Earth and Planetary Science Letters, 433, 159–168.

Kono, Y., Higo, Y., Ohfuji, H., Inoue, T., and Irifune, T. (2007). Elastic Wave Velocities of Garnetite with a MORB Composition up to 14 GPa. Geophysical Research Letters, 34(14): L14308

Kono, Y., S. Gréaux, Y. Higo, H. Ohfuji, and T. Irifune (2010), Pressure and temperature dependences of elastic properties of grossular garnet up to 17 GPa and 1650 K, Journal Earth Science, **21**, 782–791,

Kono Y, Irifune T, Ohfuji H, Higo Y, Funakoshi K-I (2012) Sound velocities of MORB and absence of a basaltic layer in the mantle transition region. Geophysical Research Letters, 39, L24306.

Larson, A.C., Von, Dreele R.B. (2000) GSAS general structure analysis system operation manual. Los Alamos National Laboratory Report LAUR, 86-748, 1-179.

Le Bail A, Duroy H, Fourquet JL (1988) Ab initio structure determination of $LiSbWO_6$ by X-ray powder diffraction. Materials Research Bulletin, 23, 447-452.

Li, B. Chen, K., Kung, J., Liebermann, R. C., and Weidner, D. J. (2002) Sound velocity measurement using transfer function method, Journal of Physics: Condensed Matter, 14, 11337-11342.

Li, L., Weidner, D.J., Brodholt, J. and Price, G.D. (2007) The effect of cation-ordering on elastic properties of majorite: An ab initio study, Earth and Planetary Science Letters, 256, 28–35.

Liu, J., Chen, G., Gwanmesia, G. D., and Liebermann, R. C. (2000) Elastic wave velocities of pyrope–majorite garnets ($Py_{62}Mj_{38}$ and $Py_{50}Mj_{50}$) to 9 GPa, Physics of the Earth and Planetary Interiors, 120,153-163.

Liu, Z., Irifune, T., Gréaux, S., Arimoto, T., Shinmei, T., and Higo, Y. (2015) Elastic wave velocity of polycrystalline $Mj_{80}Py_{20}$ garnet to 21 GPa and 2000 K, Physics and Chemistry of Minerals, 42, 213–222.

Liu, Z., Du, W., Shinmei, T., Gréaux, S., Zhou, C., Arimoto, T. Kunimoto, and T., Irifune, T. (2017) Garnets in the majorite-pyrope system: symmetry, lattice microstrain, and order-disorder of cations, Physics and Chemistry of Minerals, 4, 237-245.

Novak, G. A. and Gibbs, G. V. (1971) The crystal chemistry of the silicate garnets. American Mineralogist, 56, 791–825.

Pacalo, R. E. G. and Weidner, D. J. (1997) Elasticity of majorite, $MgSiO_3$ tetragonal garnet, Physics of the Earth and Planetary Interior*s*, 99, 145-154.

Pamato, M. G., Kurnosov, A., Boffa Ballaran, T. B., Frost, D. J., Ziberna, L., Giannini, M., Speziale, S., Tkachev, S. N., Zhuravlev, K. K., and Prakapenka, V. B. (2016) Single-crystal elasticity of majoritic garnets: stagnant slabs and thermal anomalies at the base of the transition zone, Earth and Planetary Science Letters, 451, 114–124.

Parise, J. B., Wang, Y., Gwanmesia, G.D., Zhang, J., Sinelnikov, Y., Chmielowski, J., Weidner, D.J., and Liebermann, R.C. (1996) The symmetry of garnets on the pyrope ($Mg_3Al_2Si_3O_{12}$) - majorite ($MgSiO_3$) join. Geophysical Research Letters, 23, 3799–3802

Rigden, S. M. Gwanmesia, G. D. and Liebermann, R. C. (1994) Elastic wave velocities of a pyrope-majorite garnet to 3 GPa, Physics of the Earth and Planetary Interiors, 86, 35-44.

Ringwood, A. E., and Major, A. (1971) Synthesis of majorite and other high pressure garnets and perovskites. Earth and Planetary Science Letters, 12: 411–418.

Shannon, R.D. (1976) Revised effective ionic radii and systematic studies of interatomic distances in halides and chalcogenides. Acta Crystallographica A, 32, 751–767.

Sinogeikin, S. V., Bass, J. D., O'Neill, B., and Gasparik, T. (1997) Elasticity of tetragonal end-member majorite and solid solution in the system $Mg_4Si_4O_{12}$-$Mg_3Al_2Si_3O_{12}$. Physics and Chemistry of Minerals, 24, 115-121.

Sinogeikin, S. V., and Bass, J. D., (2002a) Elasticity of Majorite and Majorite-Pyrope solid solution to high pressure: Implicaitions for the Transition Zone. Geophysical Research Letters, 9, 2453-2456.

Sinogeikin, S. V., and Bass, J. D., (2002b) Elasticity of pyrope and majorite-pyrope solid solutions to high temperatures, Earth and Planetary Science Letters, 203, 549-555.

Wang, Z. M and Ji, S. (2001) Elasticity of six polycrystalline silicate garnets at pressure up to 3.0 GPa. American Mineralogist, 86, 1209-1218

Yeganeh-Haeri, A. Weidner, D. J., and Ito, E. (1990) Elastic properties of the pyrope-majorite solid solution series, Geophysical Research Letters, 17, 2453-2456.

Zhou, C., Gréaux, S., Nishiyama, N., Irifune, T., Higo, Y. (2014) Sound velocities measurement on $MgSiO_3$ akimotoite at high pressures and high temperatures with simultaneous in situ X-ray diffraction and ultrasonic study. Physics of the Earth and Planetary Interiors, 228, 97-105.

Zou, Y., Irifune, T., Gréaux S., Whitaker, M. L., Shinmei, T., Ohfuji H., Negishi, R., and Higo, Y. (2012) Elasticity and sound velocities of polycrystalline $Mg_3Al_2(SiO_4)_3$ garnet up to 20 GPa and 1700 K, Journal of Applied Physics, 112, 014910.

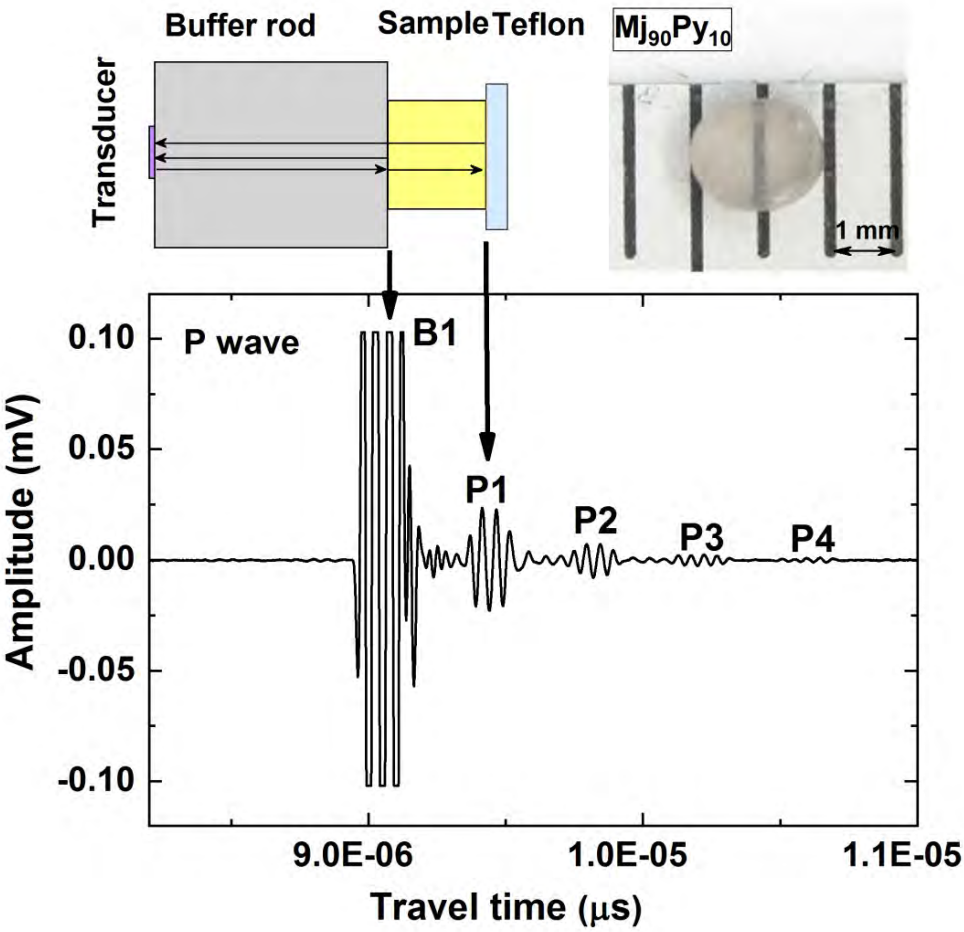

Figure 1. Schematic diagram for ultrasonic interferometric measurements on one $Mj_{90}Py_{10}$ garnet and the waveform data for P- wave for 60 MHz at ambient condition. B1 wave represents the wave echo from the interface of buffer rod, while P1-4 waves represent the echo trains from the interface of bottom sample.

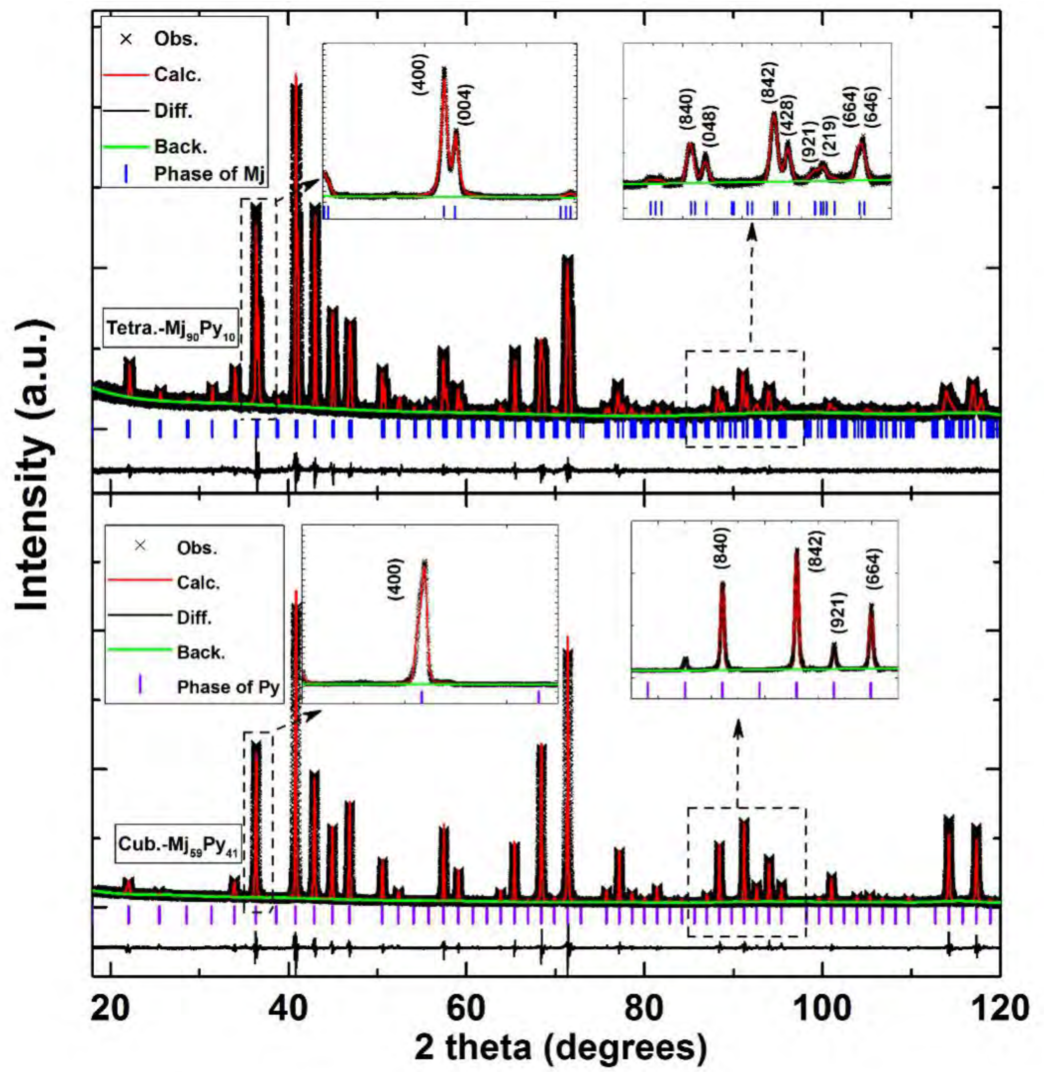

Figure 2. Representative XRD profiles of one tetragonal ($Mj_{90}Py_{10}$, top) and one cubic ($Mj_{59}Py_{41}$, bottom) garnet. Crosses represent the experimental data and red solid lines represent the fitting results using LeBail methods (Le Bail et al. 1988) with the multi-phase profile-fitting technique implemented in the EXPGUI/GSAS software package (Larson and Von Dreele 2000). The difference between calculated and observed intensities is shown below the diffraction pattern. blue and purple lines represent the (hkl) reflections of the tetragonal $MgSiO_3$ majorite (Angel et al., 1989) and cubic pyrope (Hazen and Finger, 1978), respectively.

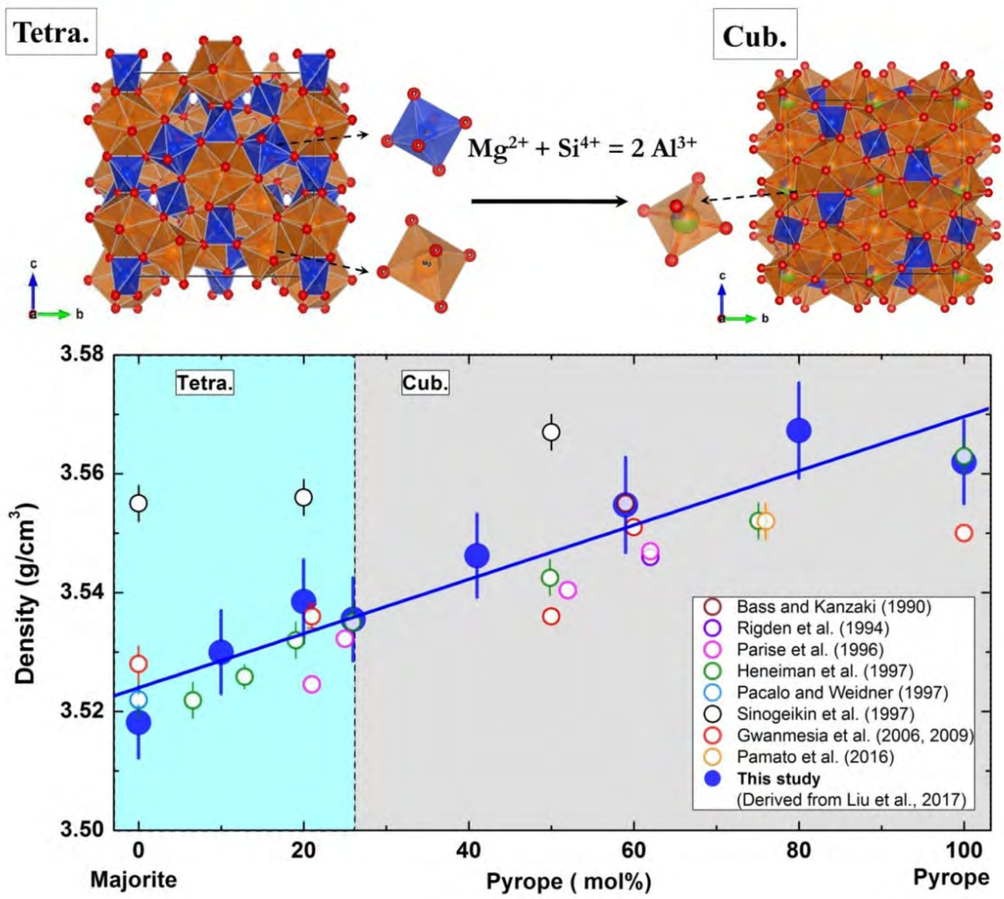

Figure 3. Crystallographic structure of one cubic and one tetragonal garnet (yellow, blue, green, and red circles present Mg, Si, Al, and O atoms) and density of majorite-pyrope garnets in the present and previous studies. The blue shadow region represents the compositions where the tetragonal (Tetra) structure is stable while the grey shadow region represents the compositions for the cubic (Cub) garnets.

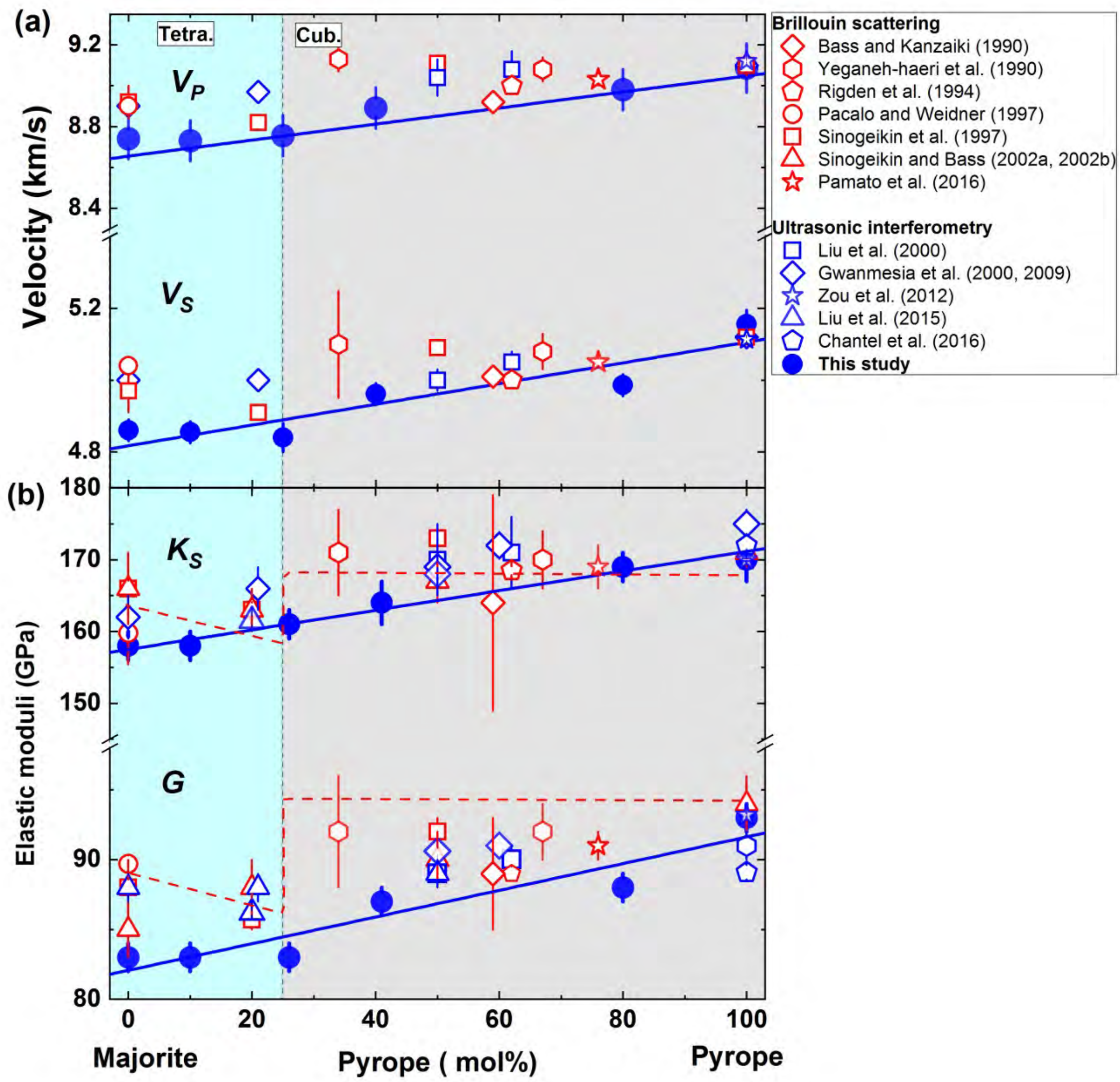

Figure 4. (a) Elastic velocities for compression (V_P) and shear (V_S) wave and (b) bulk (K_S) and shear (G) moduli as a function of the pyrope content along the majorite-pyrope system at ambient conditions. Blue-shadow regions represent the tetragonal garnets, while grey-shadow regions represent the cubic garnets. Blue solid lines are the linear fitting of the present data, while red dashed lines are the results suggested by Sinogeikin et al. (1997).

This is a preprint, the final version is subject to change, of the American Mineralogist (MSA)
Cite as Authors (Year) Title. American Mineralogist, in press.
DOI: https://doi.org/10.2138/am-2019-6771

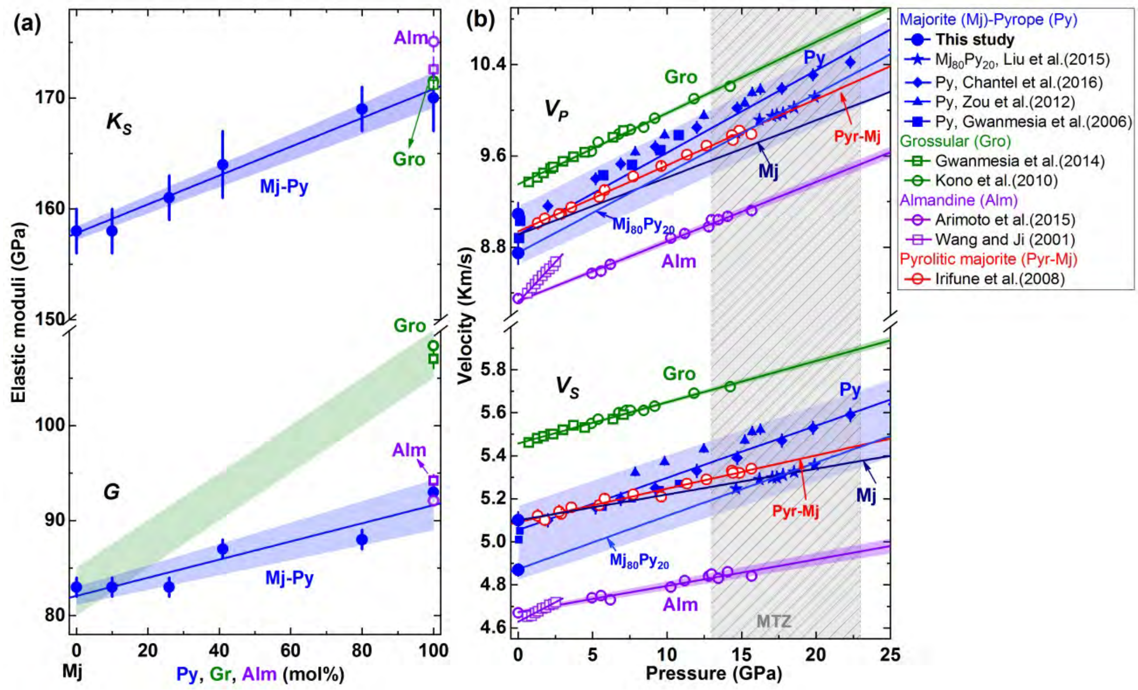

Figure 5. (a) Bulk (K_S) and shear (G) modulus of majorite-pyrope garnets in the present study together with almandine (Wang and Ji, 2000; Arimoto et al., 2015) and grossular (Kono et al., 2010; Gwanmesia et al., 2014) in previous studies at ambient conditions. (b) Sound velocity of V_P and V_S of majorite-pyrope garnets (ambient conditions, this study), pyrope (Gwanmeia et al., 2006; Zou et al., 2012; Chantel et al., 2016), $Mj_{80}Py_{20}$ (Liu et al., 2015), majorite (Zhou et al., 2014), grossular (Kono et al., 2010, Gwanmeia et al., 2014), almandine (Arimoto et al., 2015), and pyrolitic majorite (Irifune et al., 2008) at pressures up to mantle transition zone conditions (MTZ, sparse grey shadow). Solid lines are the linear fitting of the current reported data in previous studies. Shadows are the uncertainties of elastic moduli and velocities.

DOI: https://doi.org/10.2138/am-2019-6771

Table 1. Density, velocity, and elastic modulus of majorite-pyrope garnets.

Comp.	ρ (g/cm^3)	V_P (km/s)	V_S (m/s)	K_S (GPa)	G (GPa)
Pyrope	3.562 (7)	9.09 (12)	5.10 (4)	170 (3)	93 (1)
$Mj_{20}Py_{80}$	3.567 (8)	8.98 (8)	4.99 (3)	169 (2)	88 (1)
$Mj_{59}Py_{41}$	3.546 (8)	8.89 (12)	4.96 (3)	164 (3)	87 (1)
$Mj_{74}Py_{26}$	3.535 (7)	8.76 (10)	4.87 (4)	161 (2)	83 (1)
$Mj_{90}Py_{10}$	3.530 (7)	8.73 (10)	4.86 (3)	158 (2)	83 (1)
Majorite	3.518 (6)	8.74 (10)	4.86 (3)	158 (2)	83 (1)

Notes: Density is derived from our recent study (Liu et al., 2017) .
The number in parentheses represents standard deviations for the last digit(s).
Velocity calculation and error analysis can be found in Supplemental Table S1 and text.